

Anisotropy-mediated reentrant localization

X. Deng,^{1,*} A. L. Burin,² and I. M. Khaymovich³

¹*Institut für Theoretische Physik, Leibniz Universität Hannover, Appelstr. 2, 30167 Hannover, Germany*

²*Department of Chemistry, Tulane University, New Orleans, Louisiana 70118, USA*

³*Max-Planck-Institut für Physik komplexer Systeme, Nöthnitzer Straße 38, 01187-Dresden, Germany*

(Dated: February 4, 2020)

Motivated by the recently discovered localization in disordered dipolar quantum systems, which is robust against effective power-law hopping r^{-a} of dipole-flip excitations induced by dipole-dipole interactions, we consider 2d dipolar system, $d = 2$, with the generalized dipole-dipole interaction $\sim r^{-a}$, actual for experiments on trapped ions. We show that the homogeneous tilt β of the dipoles giving rise to the anisotropic dipole exchange leads to the non-trivial delocalization and reentrant localization. We find that the Anderson transitions occur at the finite values of the tilt parameter $\beta = a$, $0 < a < d$, keeping the localization to be robust at small anisotropy values. Moreover, the localized phase is shown to extend to smaller values of $a = a_{AT}(\beta) < d$ with respect to the standard resonance counting, $a = d = 2$, and this extension is non-monotonic with respect of the tilt angle. Both extensive numerical calculations and analytical methods show power-law localized eigenstates in the bulk of the spectrum, obeying recently discovered duality $a \leftrightarrow 2d - a$ of their spatial decay rate, on the localized side of the transition, $a > a_{AT}$. This localization emerges due to the presence of the ergodic extended states at either spectral edge, which constitute a zero fraction of states in the thermodynamic limit, decaying though extremely slowly with the system size. The extended phase, $a < a_{AT}$, is characterized by the finite-size multifractality going towards ergodicity.

Introduction— With the realization of Anderson localization [1] of matter waves in optical lattice, many extensions of disordered quantum systems are proposed and implemented with and without interactions. A few of notable examples are vibrational modes of polar molecules [2], Rydberg atoms [3, 4], nitrogen vacancy centers in diamond [5], magnetic atoms [6, 7], photonic crystals [8], nuclear spins [9], trapped ions [10, 11] and Frenkel excitations [12]. In these systems power-law interactions of dipole-dipole kind controlling effective hopping of excitations are ubiquitous. In addition, in the experiments of atomic systems long-range interactions can be precisely controlled. The behavior of such systems in disordered environment is described exactly by random matrix models with power-law decaying off-diagonal elements. Recent studies show that the disordered models with fully-correlated long-range hopping are localized in 1D [13, 14]. In particular, isotropic power-law hopping models $1/r^a$ show the duality of power-law localization at $a < d$ and $a > d$ [14, 15].

However, experimentally feasible dipolar systems are also characterized by common anisotropy which may have drastically different physics from the isotropic case. Usually the anisotropic terms are considered as quasi-disorder [16–19] and may lead to the localization-delocalization transition. However, here we show that the situation is more subtle as anisotropy may give rise to the reentrant localization phase diagram, Fig 1 (b).

In this work we consider two-dimensional, $d = 2$, quantum dipolar system allowing angular anisotropy with on-site disordered chemical potential, Fig. 1(a), and show that Anderson localization is robust to the homogeneous

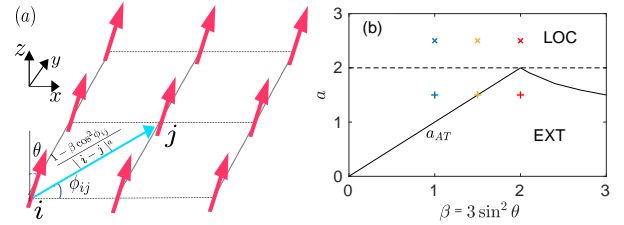


FIG. 1. Model and phase diagram. (a) Two-dimensional (2d) lattice of quantum dipoles interacting via the generalized dipole-dipole term $(1 - \beta \cos^2 \phi_{ij})/|i - j|^a$. $i = (i_x, i_y)$ is the coordinate vector of i th dipole, $a > 0$ is the effective dipole-dipole interaction exponent. The anisotropy parameter $\beta = 3 \sin^2 \theta$ is governed by the homogeneous tilt angle θ of all dipoles from the normal z -axis to the lattice plane. ϕ_{ij} is the angle between the spatial 2d vector $i - j$ and the direction of the electric field (x -axis). (b) The phase diagram of the anisotropic 2d dipole model with the on-site energy disorder. The critical line $a = a_{AT} = \min[\beta, \beta/(\beta - 1)]$ separates the localized (“LOC”) phase, $a > a_{AT}$, from the extended phase at $a < a_{AT}$. The selected points with symbols “+” and “x” of the same colors (used in further figures) indicate the duality of power-law localization of wavefunctions for $a < d = 2$ and $a > d$.

tilt of all dipoles up to a finite critical tilt value, Fig. 1(b) unlike models with disordered off-diagonal terms [20]. Moreover, we demonstrate that the anisotropy leads to the reentrant character of localization showing localized eigenstates both at small (nearly isotropic) and large (strongly anisotropic) tilt. The extensive numerical simulations showing consistent behavior of level statistics and spatial wavefunction properties are analytically supported by the renormalization group analysis (similar to [13, 21]) and the newly developed matrix inversion

* Xiaolong.Deng@itp.uni-hannover.de

trick [15]. In the extended phase eigenstates show weak multifractality which appears to be a finite-size effect, but should be visible in finite realistic systems. Experimentally the spin-models built with trapped ions in arrays of microtraps would be a feasible platform for observing such anisotropy-driven reentrant localization transition and the finite-size multifractal states.

Models and methods— We consider the model described by the Hamiltonian on a square lattice of sites $\{i = (i_x, i_y)\}$ of size L , $0 \leq i_x, i_y < L$, Fig. 1(a),

$$H = - \sum_{i,j} \frac{1 - \beta \cos^2 \phi_{ij}}{r_{ij}^a} |i\rangle \langle j| + \sum_i \mu_i |i\rangle \langle i|, \quad (1)$$

where $\{|i\rangle\}$ are site basis states, $\mu_i \in [-\frac{W}{2}, \frac{W}{2}]$ is on-site disorder uniformly distributed over the above interval, the hopping term depends on the distance $r_{ij} = \sqrt{(i_x - j_x)^2 + (i_y - j_y)^2}$ between two lattice sites and its angle ϕ_{ij} with respect to electric field x -axis. The anisotropy parameter $\beta = 3 \sin^2 \theta$ is introduced by analogy to the experimental setup of dipolar molecules, Fig. 1(a), and is related to the homogeneous tilt angle θ of dipoles w.r.t. the z -axis. In this work we restrict our consideration to the physical values of $0 \leq \beta \leq 3$ [22]

The isotropic limit, $\beta = 0$, considered in a seminal paper of one of us [13] for $a = d = 3$ and investigated in details for $d = 1$ in [14, 15] represents a newly discovered universality class of long-range models with fully-correlated hopping. It is these complete correlations that allow destructive interference of long-range hops, similarly to the standard weak and Anderson localization case, and localize the system for all values of a .

In the opposite limit of a long-range model with *fully uncorrelated random-sign* hopping h_{ij}/r_{ij}^a [16–18, 23] it is well-known that the localization occurs only for $a > d$, while the ergodic delocalization spans over the entire range $a < d$. The pure d -dimensional dipolar case of our model, $\beta = d$, (initially considered in [16–18, 24] for different d) leads to the same result, see Fig. 1(b) [25, 26].

One may naively expect that the intermediate case of $\beta \neq 0, d$ is similar to the perturbation of the fully-correlated model ($\beta = 0$) by a fraction $\epsilon \sim \beta/d$ of random-sign hopping $(1 + \epsilon h_{ij})/r_{ij}^a$ (at least for $0 < \beta < d$) as finite β works as a kind of quasi-disorder. However, in the latter model any $\epsilon > 0$ immediately delocalizes the spectral bulk states at $a < d$ as shown in [14, 20], which is not consistent with the phase diagram, Fig. 1(b).

Instead, in the anisotropic model (1) there is a *finite* tilt value $\beta_{AT}(a)$ of the Anderson transition

$$\beta_{AT} = a, \quad 0 \leq a \leq 2. \quad (2)$$

In addition, the Hamiltonian (1) obeys the 90° -rotational symmetry, $\phi_{ij} \leftrightarrow \phi_{ij} + \pi/2$, combined with the disorder strength $W \leftrightarrow W/(1 - \beta)$ and the tilt renormalization

$$\beta \leftrightarrow \frac{\beta}{\beta - 1}, \quad (3)$$

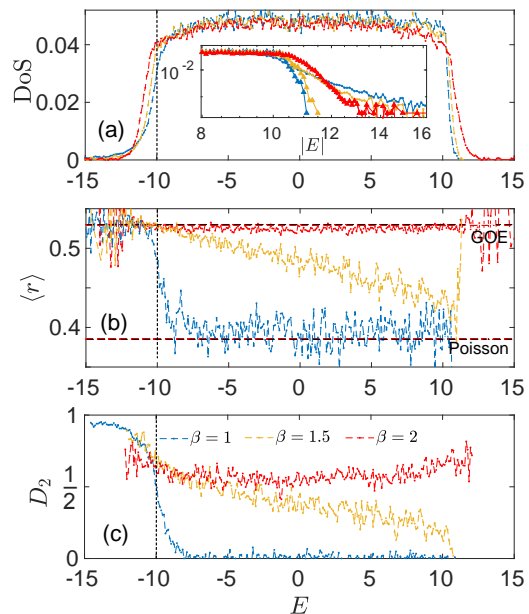


FIG. 2. Emergence of the mobility edge across the Anderson transition. (a) global density of states (DOS), (b) level-spacing ratio r -statistics, and (c) fractal dimensions D_2 for each eigenstate versus energy E in the localized ($a = 1.5, \beta = 1$, blue), critical ($a = \beta = 1.5$, yellow), and delocalized ($a = 1.5, \beta = 2$, red) phases. Both panels (b) and (c) show localized, multifractal and ergodic wavefunctions in the bulk of the spectrum. The bulk states are within the range $[-W/2, W/2]$, where we take $W = 20$. The inset to panel (a) shows power-law tails of DOS at either ($a > a_{AT}$) or both ($a < a_{AT}$) spectral edges. All the data is extrapolated from $L = 100, 150, 200$, and 250 with the corresponding number of disorder realizations 1000, 500, 100, and 50, respectively (see Appendix A 2).

which relates the interval $0 < \beta < 2$ to the ones $\beta < 0$ and $\beta > 2$ and explains the reentrant character of the above phase diagram [27]. Further for simplicity we restrict our consideration to $0 < \beta < 2$ without loss of generality.

The phase diagram, Fig. 1(b), is obtained from extensive numerical simulations. The eigenfunctions $\psi_n(i)$ and eigenenergies E_n of the Hamiltonian, Eq. (1), are numerically calculated by exact diagonalization for 2d square samples of the linear size L from 75 to 280 and for $10^2 - 10^3$ random realizations of the diagonal disorder. The ratio level statistics, Fig. 2(b)

$$r = \left\langle \min \left(r_{n,1}, \frac{1}{r_{n,1}} \right) \right\rangle, \quad r_{n,1} = \frac{E_n - E_{n-1}}{E_{n+1} - E_n} \quad (4)$$

is calculated in the bulk of the spectrum where the density of states (DOS), $\rho(E) = \langle \sum_n \delta(E - E_n) \rangle$, Fig. 2(a), is not small. The r -statistics shows the value $r = 2 \ln 2 - 1 \simeq 0.3863$ of Poisson level statistics for all spectral bulk states in the localized phase, and $r \approx 0.5307$ of Gaussian orthogonal ensemble (GOE) for the extended phase and at the spectral edge [28, 29]. The more detailed finite-size analysis of r -statistics determines the transition line $\beta = \beta_{AT}(a)$, Eq. (2), via the change of finite-size

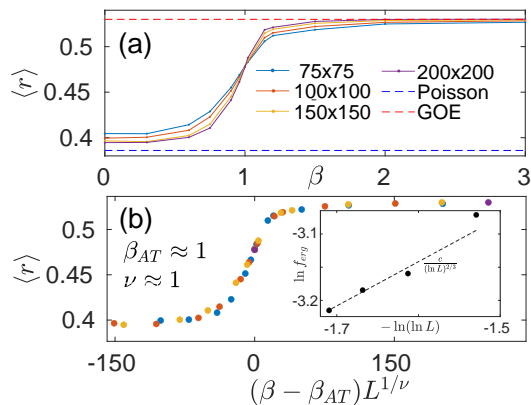


FIG. 3. **Anisotropy-driven Anderson transition and r -statistics collapse.** (a) Level statistics versus anisotropy β at $a = 1$ at system sizes shown in legend; (b) Scaling collapse of $\langle r \rangle$ using $\langle r \rangle = R [(\beta - \beta_{AT})L^{1/\nu}]$, giving $\beta_{AT} = 1.0 \pm 0.1$ and $\nu = 1.0 \pm 0.1$ for $a = 1$. The calculations of $\langle r \rangle$ are done on eigenstates from the interval $E \in [-W/2, W/2]$, $W = 20$, which constitute 95% of all the states. (inset) Fraction f_{erg} of ergodic extended states below the mobility edge, $E < E^*$, in the localized phase, $a = 1.5$, $\beta = 0.3$, versus the system size L . The number of disorder realizations is 1000 (for $L \leq 100$) 500 ($L = 150$), and 100 ($L = 200$). Scaling is consistent with analytical predictions in (8).

flow of $r(a, \beta, L)$ versus L , see Appendix A 1, Fig. 3(a). The standard collapse of $r = R [(\beta - \beta_{AT})L^{1/\nu}]$ of the finite-size r -data gives $\beta_{AT} = a$ for $0 < \beta < 2$ and $\nu \simeq 1$ for all considered a , Fig. 3(b). At the transition line the r -statistics takes the universal value $\langle r \rangle \approx 0.47$ independent of a . The fractal dimension D_2 extracted from the inverse participation ratio $I_2 = \sum_i |\psi_n(i)|^4 \propto N^{-D_2}$ shows consistent behavior in the localized ($D_2 \rightarrow 0$), critical ($0 < D_2 < 1$), and extended phases ($D_2 \rightarrow 1$), Fig. 2(c). However, in the latter case the finite-size data shows very slow convergence to 1 [30] and the simple $1/\ln N$ -extrapolation gives $D_2 \simeq 0.7$, see [31, 32] and Appendix A 2.

From the above mentioned three measures one can extract the position of a kind of the mobility edge E^* below which all the states are ergodic [27], while being power-law localized (extended with smaller extrapolated D_2) above it for $a > a_{AT}$ ($a < a_{AT}$). The finite-size analysis shows (see the inset to Fig. 3(b)) that the corresponding fraction of ergodic states $f_{\text{erg}} = \sum_{E < E^*} \rho(E)/N$ in the localized phase $\beta < a$ decays with the system size L , but does it logarithmically slowly, see Appendix A 3.

The non-trivial phase diagram and anisotropy-mediated reentrant localization transition can be understood from the atypical extended nature of edge spectral states in both isotropic, $\beta = 0$, and anisotropic, $\beta > 0$ cases of a dipole system. Indeed, due to the diverging

nature of the spectrum

$$V_q = - \int_0^\infty r dr \int_0^{2\pi} d\phi e^{iqr \cos(\phi - \phi_q)} \frac{1 - \beta \cos^2 \phi}{r^a} = c_a q^{a-2} [\beta - a - (2-a)\beta \cos^2 \phi_q], \quad (5)$$

of the hopping term $\sum_q V_q |q\rangle \langle q|$ in (1) at small $q < q_* \ll 1$ and $a < d = 2$ there are large negative energy states, $E \simeq V_q < E^* < 0$, with $|E^*| \gg W$, which are barely affected by the on-site disorder and, thus, are diffusive states represented by superpositions of plane waves with small momenta $q < q_*$. Here the hopping term is diagonalized in the momentum basis $|q\rangle = \sum_n \frac{e^{iqn}}{N^{1/2}} |n\rangle$ due to its translation invariance, c_a is a certain q -independent positive constant given in Appendix C, the momentum $\vec{q} = \frac{\pi}{L}(n_x, n_y)$ written in polar coordinates $q = \frac{\pi}{L} \sqrt{n_x^2 + n_y^2}$ and $\tan \phi_q = n_y/n_x$ is quantized in the reciprocal Brillouin zone, with integer $0 \leq n_x, n_y < L$. Although the above extended eigenstates $E_n \simeq V_q < E^* < 0$ constitute a zero fraction of all states, they give the main contribution to the hopping term

$$\sum_q V_q |q\rangle \langle q| = \sum_{E_n < E^*} E_n |E_n\rangle \langle E_n| + J_{\text{res}}. \quad (6)$$

Due to the orthogonality of the eigenbasis, the rest states $E_n > E^*$ “observe” only the residual hopping term J_{res} with substantially suppressed long-range structure and, thus, are localized. These arguments work provided the extended large-energy states appear on the only edge of the spectrum and, thus, their contribution to (6) cannot be compensated by the states from the other spectral edge. The effect of extended spectral edge states has been partially understood for the case of $a = 0$, $d = 1$ corresponding to the only extended state in terms of cooperative shielding in [33] and explained in details for the general case by the matrix inversion trick in [15, 20] and by the renormalization group in [21].

In our model (1), the sign conservation of V_q , Eq. (5),

$$a|\beta - 2| > |a - 2|\beta \quad (7)$$

immediately provides the boundary of the localized phase $\beta < \beta_{AT}(a)$, Eq. (2), for all a and β . The special structure of energies $E_n \simeq V_q \sim q^{a-2}$ at the spectral edge(s) is explicitly represented by the power-law decaying tail of DOS on either (both) edge(s) of the spectrum in the localized (extended) phase, see the inset to Fig. 2(a).

The mobility edge $E^* \simeq V_{q_*}$ found numerically can be determined by Ioffe-Regel criterion [34]. Indeed, a state is localized as soon as its localization length ℓ_{loc} is smaller than the system dimension L . In 2d systems the localization length is exponentially growing with the mean-free path $\ell_{loc} \sim e^{ck_F \ell_{mfp}}$, with a certain constant $c \sim O(1)$. Fixing a certain momentum playing a role of the Fermi momentum $k_F = q$ one calculates the mean free path as $\ell_{mfp}(q) \simeq v_q \tau_q$ via the group velocity

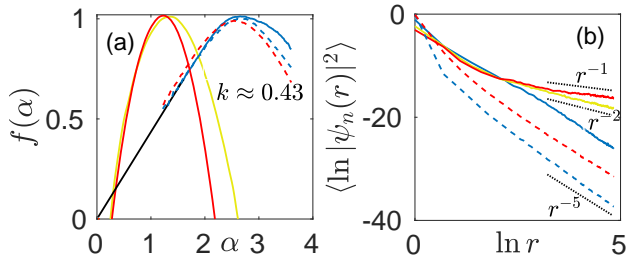


FIG. 4. **Spatial properties in the spectral bulk.** (a) spectrum of fractal dimensions $f(\alpha)$ and (b) power-law spatial decay of eigenstates in the bulk of the spectrum for $a = 1.5$ (solid), 2.5 (dashed), and $\beta = 1$ (blue), 1.5 (yellow), 2 (red). The panel (b) confirms the duality of power-law spatial decay rate $\gamma(a) \approx \gamma(2d - a)$ in the localized phase of the anisotropic model supported as well by the slope of $f(\alpha)$ in panel (a). $f(\alpha)$ is extrapolated from $L = 100, 150, 200,$ and 250 with the corresponding number of disorder realizations $1000, 500, 100,$ and $50,$ respectively, and with the disorder amplitude $W = 20$, see Appendix A 2. For the spatial decay $L = 250$ and $W = 20$ for $a = 1.5,$ for $a = 2.5$ we choose bigger $W = 200$ in order to make the power-law tail dominant on moderate sizes.

$v_q = d\tilde{V}_q/dq \sim q^{a-d-1}$ at the momentum q and the level broadening $\gamma_q = \tau_q^{-1}$ determined by the Fermi Golden rule $\gamma_q \sim W^2 \rho(E) \sim W^2 q^{2d-a}$ for the plane wave scattering on impurities $\mu_i \simeq W$. This gives the fraction f_{erg} of ergodic extended states below the mobility edge

$$f_{\text{erg}} = \pi q_*^2 \sim [W^2 \ln L]^{-1/(3-a)}, \quad (8)$$

which reduces with the system size only as a power of the logarithm, see inset to Fig. 3(b).

Focusing now on the properties of the bulk spectral states we investigate them in terms of the multifractal analysis and spatial decay in more details. Indeed, the multifractal spectrum (MFS) $f(\alpha)$, characterizing the multifractality of the states, is defined by the probability distribution $\mathcal{P}(\ln |\psi_n(i)|^2) \sim N^{f(\alpha)-1}$ of the logarithm of the wavefunction intensity $\alpha = -\ln |\psi_n(i)|^2 / \ln N$ [23] and can be extracted directly from the histogram over α [35–37]. For the non-ergodic extended states in most cases the MFS obeys a so-called Mirlin-Fyodorov symmetry $f(1 - \delta\alpha) = f(1 + \delta\alpha) - \delta\alpha$ [23]. The ergodic extended state corresponds to a δ -function at $\alpha = 1$ [38], while the localized state has $f(0) = 0$ and a certain (usually linear) form of $f(\alpha > 0) = k\alpha$, with $k = 0$ for exponential and $k > 0$ for power-law localization [39]. In the model (1) the multifractal spectrum of the bulk spectral states, Fig. 4(a), shows power-law localized ($\beta = 1$), multifractal ($\beta = 1.5$), and multifractal-to-ergodic finite-size ($\beta = 2$) behavior [30, 32] in the localized phase, at the transition, and in the extended phase, respectively.

The spatial decay $\langle \ln |\psi_n(i)|^2 \rangle$ of the typical wavefunction intensity $|\psi_n(i)|^2$ with the distance $r = |i - i_0|$ from its maximum $i = i_0$ suggested as the localization measure in [14] and used in [15, 20, 21] shows the same duality of

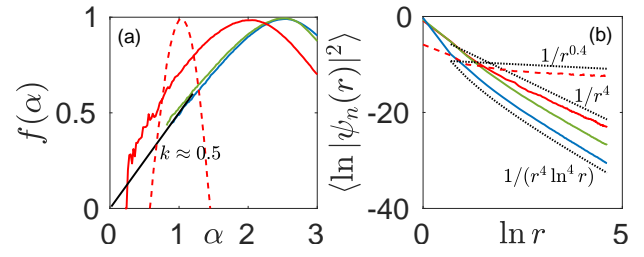


FIG. 5. **Multifractal properties at the dual line $a = d = 2$.** (a) spectrum of fractal dimensions $f(\alpha)$ and (b) power-law spatial decay of eigenstates in the bulk of the spectrum at the self-dual line $a = 2$ of (9) for $\beta = 1$ (blue), 2 (red), 3 (green). The linear behavior of $f(\alpha)$ with the slope close to $k = 0.5$ supports the critical localization for $\beta \neq 2$. The exceptional point $a = \beta = 2$ shows the transition from ergodicity ($W = 4$, dashed) to localization ($W = 40$, solid) over the disorder amplitude. The disorder strength for $\beta = 1, 3$ is $W = 40$. $f(\alpha)$ is extrapolated from $L = 100, 150, 200,$ and 250 with the corresponding number of disorder realizations $1000, 500, 100,$ and $50,$ respectively, see Appendix A 2. For the spatial decay $L = 200$.

the power-law decay rate

$$|\psi_n(i)| \sim r^{-a} \text{ for } a > d \quad (9a)$$

$$|\psi_n(i)| \sim r^{a-2d} \text{ for } a < d \quad (9b)$$

as in [14, 15, 21], Fig. 4(b), in the whole range of anisotropy parameter β in the localized phase. In the extended phase the dual power-law decay develops at finite small distances, but becomes extended $|\psi_n(i)| \sim N^{-s} r^{-c}$, $c \leq d$, $s > 0$, at larger distances, see Appendix B. These power-law tails do not lead to the wavefunction localization with $\psi_n(i_0) \sim O(1)$. Instead it gives $|\psi_n(i_0)|^2 \sim L^{-ds}$ and the typical value $|\psi_n(L)|^2 \sim L^{-(c+sd)}$ with $c + sd \rightarrow d$ in the thermodynamic limit $N \rightarrow \infty$. Thus, we have to conclude only finite-size multifractality tending toward ergodicity [30, 32].

At the self-dual line $a = d = 2$ of (9) the wavefunction behavior is consistent with the critical localization, Fig. 5, $f(\alpha) \simeq k\alpha$, with $k = 1/2$ corresponding to the localized eigenstate, but still obeying the Mirlin-Fyodorov symmetry [23], with the spatial decay [21]

$$|\psi_n(i)| \sim r^{-d} (\ln r)^{-2}. \quad (10)$$

The pure 2d dipole point $a = \beta = 2$ considered in [24] and revisited in [31] is exempted here as it shows the transition from ergodicity to localization over the disorder amplitude.

Both (9) and (10) can be understood in terms of the renormalization group (RG) analysis similar to the one done in [13, 21]. The main assumption of the RG written in the limit of large disorder strength $W \gg 1$ is that at each step over the hopping radius R , taken into account at this step, the localization lengths ℓ^R of the states $|\psi_n^R\rangle = \sum_i \psi_n^R(i) |i\rangle$ around their maximum $i = n$ are small compared to R . This allows to take into account

only resonant pairs and approximate the renormalized hopping potential as follows

$$\sum_{i,j} \frac{1 - \beta \cos^2 \phi_{ij}}{r_{ij}^a} |i\rangle\langle j| \simeq \sum_{n,m} l_n l_m \frac{1 - \beta \cos^2 \phi_{mn}}{r_{mn}^a} |\psi_m^R\rangle\langle\psi_n^R|, \quad (11)$$

with $l_n = \sum_i \psi_n^R(i)$ [40].

The upper estimate of the renormalization prefactor $l_n l_m$ at a certain energy $E_n, E_m \simeq E$ can be written as

$$\begin{aligned} \langle l^2 \rangle_E &= \frac{\langle \sum_n l_n^2 \delta(E - E_n) \rangle}{\rho(E)} \simeq \frac{\sum_{|m-n| < R} \langle \text{Im } G_{m-n} \rangle}{\pi \rho(E)} \\ &\simeq \frac{\text{Im } \bar{G}_{|q| \simeq 1/R}(E)}{\pi \rho(E)}, \quad (12) \end{aligned}$$

via DOS and the Green function $\bar{G}_q(E)$ averaged of the on-site disorder. The latter reads as $\bar{G}_q(E) = [E - V_q - \Sigma]^{-1}$, with the self-energy given by a simplest coherent potential approximation $\Sigma = -\frac{W^2}{12} \bar{G}_0(E)$, consistent with the Fermi Golden rule result $\text{Im } \Sigma = -\gamma_q$. At small energies $E \sim W$ DOS is determined by the disorder $\rho(E) \sim 1/W$ and thus

$$\begin{aligned} \langle l^2 \rangle_E &= \frac{W}{2\pi^2} \text{Im} \int_0^{2\pi} \frac{d\phi_q}{E - V_q - \Sigma} = \\ &\frac{W}{2\pi^2} \int_0^{2\pi} \frac{\gamma_q d\phi_q}{(E - V_q - \text{Re } \Sigma)^2 + \gamma_q^2}. \quad (13) \end{aligned}$$

At $a < d$ the integrand denominator is dominated by the hopping spectrum, V_q , so the angle averaging depends on whether V_q versus ϕ_q changes the sign or not for $q \simeq 1/R \ll 1$.

For sign-invariant V_q , Eq. (7), the integral is given mostly by $\langle l^2 \rangle_E \sim W \gamma_q / V_q^2 \simeq 1/R \sim R^{2(a-d)}$ and leads

to (9b). This result can be equivalently obtained from the matrix-inversion trick [15]. More rigorous calculations done at $a = d = 2$ [21] and Appendix D give logarithmic corrections leading to (10). In the opposite case of $a < a_{AT}$, V_q changes sign w.r.t. ϕ_q and simple calculations give $\langle l^2 \rangle_E \sim W/V_q \simeq 1/R \sim R^{a-d}$ resulting in $|\psi_E(i)|^2 \sim r^{-d}$. This critical behavior, formally equivalent to the critical case of $a = d$ for the random-sign hopping term h_{ij}/r_{ij}^a , hints that the delocalized phase at $a < a_{AT}$ is nonergodic. However, more rigorous calculations of transport based on Kubo formula [31] give logarithmic corrections leading to ergodic behavior.

To sum up, we explicitly show both numerically and analytically the phenomenon of the anisotropy-mediated reentrant Anderson localization transition in 2d quantum dipole model. The transition is demonstrated to occur at a finite anisotropy tilt angle of dipoles depending on the exponent a of the generalized dipole-dipole interaction controlling excitation hopping. Moreover, close to the pure 2d dipole-dipole interaction $1 < a \leq 2$ the phase diagram has a reentrant nature showing the localization both at large and small tilts.

It might be interesting to include the interactions between excitations in the model, to see whether there is a many-body localization transition driven by the anisotropy of long-range couplings [41–53]

ACKNOWLEDGMENTS

We thank V. E. Kravtsov for illuminating discussions. We also thank G. V. Shlyapnikov and Luis Santos for previous collaboration on related topics. This research was supported by the DFG projects SA 1031/11, SFB 1227 DQ-mat (X. D.), KH 425/1-1 (I. M. K.), and by the Russian Foundation for Basic Research Grant No. 17-52-12044 (I. M. K.).

-
- [1] P. W. Anderson, “Absence of diffusion in certain random lattices,” *Phys. Rev.* **109**, 1492 (1958).
- [2] Bo Yan, Steven A Moses, Bryce Gadow, Jacob P Covey, Kaden RA Hazzard, Ana Maria Rey, Deborah S Jin, and Jun Ye, “Observation of dipolar spin-exchange interactions with lattice-confined polar molecules,” *Nature* **501**, 521 (2013).
- [3] Johannes Zeiher, Jae-yoon Choi, Antonio Rubio-Abadal, Thomas Pohl, Rick van Bijnen, Immanuel Bloch, and Christian Gross, “Coherent many-body spin dynamics in a long-range interacting ising chain,” *Phys. Rev. X* **7**, 041063 (2017).
- [4] Sylvain de Léséleuc, Vincent Lienhard, Pascal Scholl, Daniel Barredo, Sebastian Weber, Nicolai Lang, Hans Peter Büchler, Thierry Lahaye, and Antoine Browaeys, “Observation of a symmetry-protected topological phase of interacting bosons with rydberg atoms,” *Science* **365**, 775–780 (2019).
- [5] Gerald Waldherr, Y Wang, S Zaiser, M Jamali, T Schulte-Herbrüggen, H Abe, T Ohshima, J Isoya, JF Du, P Neumann, *et al.*, “Quantum error correction in a solid-state hybrid spin register,” *Nature* **506**, 204 (2014).
- [6] A. de Paz, A. Sharma, A. Chotia, E. Maréchal, J. H. Huckans, P. Pedri, L. Santos, O. Gorceix, L. Vernac, and B. Laburthe-Tolra, “Nonequilibrium quantum magnetism in a dipolar lattice gas,” *Phys. Rev. Lett.* **111**, 185305 (2013).
- [7] S. Baier, M. J. Mark, D. Petter, K. Aikawa, L. Chomaz, Z. Cai, M. Baranov, P. Zoller, and F. Ferlaino, “Extended bose-hubbard models with ultracold magnetic atoms,” *Science* **352**, 201–205 (2016).
- [8] C.-L. Hung, Alejandro González-Tudela, J. Ignacio Cirac, and H. J. Kimble, “Quantum spin dynamics with pairwise-tunable, long-range interactions,” *Proceedings of the National Academy of Sciences* **113**, E4946–E4955 (2016).
- [9] Gonzalo A. Álvarez, Dieter Suter, and Robin Kaiser,

- “Localization-delocalization transition in the dynamics of dipolar-coupled nuclear spins,” *Science* **349**, 846–848 (2015).
- [10] Philip Richerme, Zhe-Xuan Gong, Aaron Lee, Crystal Senko, Jacob Smith, Michael Foss-Feig, Spyridon Michalakis, Alexey V Gorshkov, and Christopher Monroe, “Non-local propagation of correlations in quantum systems with long-range interactions,” *Nature* **511**, 198 (2014).
- [11] Petar Jurcevic, Ben P Lanyon, Philipp Hauke, Cornelius Hempel, Peter Zoller, Rainer Blatt, and Christian F Roos, “Quasiparticle engineering and entanglement propagation in a quantum many-body system,” *Nature* **511**, 202 (2014).
- [12] Semion K Saikin, Alexander Eisfeld, Stéphanie Valleau, and Alán Aspuru-Guzik, “Photonics meets excitonics: natural and artificial molecular aggregates,” *Nanophotonics* **2**, 21–38 (2013).
- [13] A. L. Burin and L. A. Maksimov, “Localization and delocalization of particles in disordered lattice with tunneling amplitude with r^{-3} decay,” *JETP Lett.* **50**, 338 (1989).
- [14] X. Deng, V. E. Kravtsov, G. V. Shlyapnikov, and L. Santos, “Duality in power-law localization in disordered one-dimensional systems,” *Phys. Rev. Lett.* **120**, 110602 (2018).
- [15] P. A. Nosov, I. M. Khaymovich, and V. E. Kravtsov, “Correlation-induced localization,” *Physical Review B* **99**, 104203 (2019).
- [16] L. S. Levitov, “Absence of localization of vibrational modes due to dipole-dipole interaction,” *Europhys. Lett.* **9**, 83 (1989).
- [17] L. S. Levitov, “Delocalization of vibrational modes caused by electric dipole interaction,” *Phys. Rev. Lett.* **64**, 547 (1990).
- [18] L.S. Levitov, “Critical hamiltonians with long range hopping,” *Annalen der Physik* **8**, 697–706 (1999).
- [19] J. T. Cantin, T. Xu, and R. V. Krems, “Effect of the anisotropy of long-range hopping on localization in three-dimensional lattices,” *Phys. Rev. B* **98**, 014204 (2018).
- [20] P. A. Nosov and I. M. Khaymovich, “Robustness of delocalization to the inclusion of soft constraints in long-range random models,” *Phys. Rev. B* **99**, 224208 (2019).
- [21] A. G. Kutlin and I. M. Khaymovich, “Renormalization to localization without a small parameter,” (2020), [arXiv:2001.06493](https://arxiv.org/abs/2001.06493).
- [22] Note that $\beta = 0$ corresponds to the isotropic case of 3d dipoles perpendicular to the 2d plane, while $\beta = 3$ leads to the in-plane dipole moments. The case of purely 2d dipoles corresponds to $a = \beta = 2$ [24]. Mathematically, however, the whole range $\beta \in (-\infty, \infty)$ and negative a are also interesting.
- [23] F. Evers and A. D. Mirlin, “Anderson transitions,” *Rev. Mod. Phys.* **80**, 1355 (2008).
- [24] I. L. Aleiner, B. L. Altshuler, and K. B. Efetov, “Localization and critical diffusion of quantum dipoles in two dimensions,” *Phys. Rev. Lett.* **107**, 076401 (2011).
- [25] However, in a recent paper of two of authors [31] it has been shown that the critical point $a = \beta = d = 2$ corresponds to the mobility edge between ergodic and localized states in energy and in the disorder amplitude, but not to the multifractal eigenstates as claimed in [24].
- [26] A simple explanation of the equivalence of dipole-dipole induced hopping and the random-sign case is related to the fact that hopping term averages to zero over the angle ϕ_{ij} at $\beta = d$.
- [27] The change of the disorder amplitude sign with respect to the symmetry $W \leftrightarrow W/(1 - \beta)$ at $\beta > 1$ corresponds simply to mirroring of the spectrum and moving of the extended ergodic states from the bottom to the top of the spectrum.
- [28] Vadim Oganesyan and David A. Huse, “Localization of interacting fermions at high temperature,” *Phys. Rev. B* **75**, 155111 (2007).
- [29] Y. Y. Atas, E. Bogomolny, O. Giraud, and G. Roux, “Distribution of the ratio of consecutive level spacings in random matrix ensembles,” *Phys. Rev. Lett.* **110**, 084101 (2013).
- [30] Here one should distinguish finite-size multifractality going to ergodicity from a (probably) weaker phenomenon of weak ergodicity. In the latter the fractal dimensions $D_q \rightarrow 1$ also converges to one, but along the path different from the ones from the random-matrix theory, due to the occupation of only a finite fraction of the total Hilbert space by eigenstates. This phenomenon has been considered, e.g., in [15, 20, 37, 54–56].
- [31] X. Deng and A. L. Burin, (2020), in preparation (unpublished).
- [32] Unlike the long-range static [57–59] and short-range driven [60] models with correlated (quasiperiodic) onsite disorder, in the current model multifractality does not emerge in the extended phase due to the mixture of localized and ergodic states, .
- [33] G. L. Celardo, R. Kaiser, and F. Borgonovi, “Shielding and localization in the presence of long-range hopping,” *Phys. Rev. B* **94**, 144206 (2016).
- [34] Please see Appendix E. More rigorous calculations are done with help of Kubo formula in [31].
- [35] A. De Luca, B L Altshuler, V E Kravtsov, and A Scardicchio, “Anderson localization on the bethe lattice: Non-ergodicity of extended states,” *Phys. Rev. Lett.* **113**, 046806 (2014).
- [36] V. E. Kravtsov, I. M. Khaymovich, E. Cuevas, and M. Amini, “A random matrix model with localization and ergodic transitions,” *New J. Phys.* **17**, 122002 (2015).
- [37] David J Luitz, Ivan Khaymovich, and Yevgeny Bar Lev, “Multifractality and its role in anomalous transport in the disordered xxz spin-chain,” (2019), [arXiv:1909.06380](https://arxiv.org/abs/1909.06380).
- [38] With the additional tail $f(\alpha) = (3 - \alpha)/2$ for $\alpha > 1$ due to the statistics of de Broglie-like oscillations of ψ_n , see, e.g., the Supplemental Information in [35] and [37] for details.
- [39] Note that $k = 1/2$ corresponds to the critical localization as $f(\alpha) = \alpha/2$ in this case still obeys the Mirlin-Fyodorov symmetry [23].
- [40] In this approximation we neglect the difference between bare hopping terms at the distance r_{ij} and r_{mn} due to smallness of $|r_{ij} - r_{mn}| < r_{in} + r_{jm} < 2\ell^R \ll R$. Please see Appendix D for more details.
- [41] A. L. Burin and Yu. Kagan, “Low-energy collective excitations in glasses. new relaxation mechanism for ultralow temperatures,” *Zh. Eksp. Teor. Fiz.* **106**, 633 (1994).
- [42] N. Y. Yao, C. R. Laumann, S. Gopalakrishnan, M. Knap, M. Müller, E. A. Demler, and M. D. Lukin, “Many-body localization in dipolar systems,” *Phys. Rev. Lett.* **113**, 243002 (2014).
- [43] R. Singh, R. Moessner, and D. Roy, “Effect of long-range hopping and interactions on entanglement dy-

- namics and many-body localization,” *Phys. Rev. B* **95**, 094205 (2017).
- [44] D. J. Luitz and Y. Bar Lev, “Emergent locality in systems with power-law interactions,” *Phys. Rev. A* **99**, 010105(R) (2019).
- [45] T. Botzung, D. Vodola, P. Naldesi, M. Müller, E. Ercolessi, and G. Pupillo, “Algebraic localization from power-law interactions in disordered quantum wires,” (2018), [arXiv:1810.09779](https://arxiv.org/abs/1810.09779).
- [46] Sthitadhi Roy and David E. Logan, “Self-consistent theory of many-body localisation in a quantum spin chain with long-range interactions,” *SciPost Phys.* **7**, 42 (2019).
- [47] Sabyasachi Nag and Arti Garg, “Many-body localization in the presence of long-range interactions and long-range hopping,” *Phys. Rev. B* **99**, 224203 (2019).
- [48] A. L. Burin, “Many-body delocalization in a strongly disordered system with long-range interactions: Finite-size scaling,” *Phys. Rev. B* **91**, 094202 (2015).
- [49] A. L. Burin, “Localization in a random xy model with long-range interactions: Intermediate case between single-particle and many-body problems,” *Phys. Rev. B* **92**, 104428 (2015).
- [50] I. V. Gornyi, A. D. Mirlin, D. G. Polyakov, and A. L. Burin, “Spectral diffusion and scaling of many-body delocalization transitions,” *Annalen der Physik* **529**, 1600360 (2017).
- [51] K. S. Tikhonov and A. D. Mirlin, “Many-body localization transition with power-law interactions: Statistics of eigenstates,” *Phys. Rev. B* **97**, 214205 (2018).
- [52] G. De Tomasi, “Algebraic many-body localization and its implications on information propagation,” *Phys. Rev. B* **99**, 054204 (2019).
- [53] Xiaolong Deng, Guido Masella, Guido Pupillo, and Luis Santos, “Universal algebraic growth of entanglement entropy in many-body localized systems with power-law interactions,” (2019), [arXiv:1912.08131](https://arxiv.org/abs/1912.08131).
- [54] E. Bogomolny and M. Sieber, “Power-law random banded matrices and ultrametric matrices: Eigenvector distribution in the intermediate regime,” *Phys. Rev. E* **98**, 042116 (2018).
- [55] I. M. Khaymovich, M. Haque, and P. A. McClarty, “Eigenstate thermalization, random matrix theory, and behemoths,” *Phys. Rev. Lett.* **122**, 070601 (2019).
- [56] Arnd Bäcker, Masudul Haque, and Ivan M Khaymovich, “Multifractal dimensions for random matrices, chaotic quantum maps, and many-body systems,” *Phys. Rev. E* **100**, 032117 (2019).
- [57] J. Biddle, D.J. Priour, B. Wang, and S. Das Sarma, “Localization in one-dimensional lattices with non-nearest-neighbor hopping: Generalized Anderson and Aubry-André models,” *Phys. Rev. B* **83**, 075105 (2011).
- [58] S. Gopalakrishnan, “Self-dual quasiperiodic systems with power-law hopping,” *Phys. Rev. B* **96**, 054202 (2017).
- [59] X. Deng, S. Ray, S. Sinha, G. V. Shlyapnikov, and L. Santos, “One-dimensional quasicrystals with power-law hopping,” *Phys. Rev. Lett.* **123**, 025301 (2019).
- [60] S. Roy, I. M. Khaymovich, A. Das, and R. Moessner, “Multifractality without fine-tuning in a floquet quasiperiodic chain,” *SciPost Phys.* **4**, 25 (2018).
- [61] F. Evers, A. Mildenberger, and A. D. Mirlin, “Multifractality of wave functions at the quantum hall transition revisited,” *Phys. Rev. B* **64**, 241303 (2001).
- [62] Y Y Atas, E Bogomolny, O Giraud, P Vivo, and E Vivo, “Joint probability densities of level spacing ratios in random matrices,” *Journal of Physics A: Mathematical and Theoretical* **46**, 355204 (2013).
- [63] S. Harshini Tekur, Udaysinh T. Bhosale, and M. S. Sathnam, “Higher-order spacing ratios in random matrix theory and complex quantum systems,” *Phys. Rev. B* **98**, 104305 (2018).
- [64] E. Cuevas and V. E. Kravtsov, “Two-eigenfunction correlation in a multifractal metal and insulator,” *Phys. Rev. B* **76**, 235119 (2007).
- [65] Yan V. Fyodorov and Alexander D. Mirlin, “Strong eigenfunction correlations near the anderson-localization transition,” *Phys. Rev. B* **55**, R16001–R16004 (1997).
- [66] G. De Tomasi, M. Amini, S. Bera, I. M. Khaymovich, and V. E. Kravtsov, “Survival probability in generalized rosenzweig-porter random matrix ensemble,” *SciPost Phys.* **6**, 014 (2019).
- [67] S. Bera, G. De Tomasi, I. M. Khaymovich, and A. Scardicchio, “Return probability for the anderson model on the random regular graph,” *Physical Review B* **98**, 134205 (2018).
- [68] Giuseppe De Tomasi, Soumya Bera, Antonello Scardicchio, and Ivan M. Khaymovich, “Sub-diffusion in the Anderson model on random regular graph,” (2019), accepted for publication in PRB(R), [arXiv:1908.11388](https://arxiv.org/abs/1908.11388).
- [69] E. J. Torres-Herrera and Lea F. Santos, “Dynamics at the many-body localization transition,” *Phys. Rev. B* **92**, 014208 (2015).
- [70] F. Borgonovi, F.M. Izrailev, L.F. Santos, and V.G. Zelevinsky, “Quantum chaos and thermalization in isolated systems of interacting particles,” *Physics Reports* **626**, 1 – 58 (2016), quantum chaos and thermalization in isolated systems of interacting particles.
- [71] J.T. Chalker, “Scaling and eigenfunction correlations near a mobility edge,” *Physica A: Statistical Mechanics and its Applications* **167**, 253 – 258 (1990).
- [72] V. E. Kravtsov and K. A. Muttalib, “New class of random matrix ensembles with multifractal eigenvectors,” *Phys. Rev. Lett.* **79**, 1913–1916 (1997).
- [73] V. E. Kravtsov, A. Ossipov, O. M. Yevtushenko, and E. Cuevas, “Dynamical scaling for critical states: Validity of chalker’s ansatz for strong fractality,” *Phys. Rev. B* **82**, 161102 (2010).
- [74] M. Pino, V. E. Kravtsov, B. L. Altshuler, and L. B. Ioffe, “Multifractal metal in a disordered josephson junctions array,” *Phys. Rev. B* **96**, 214205 (2017).
- [75] F. A. B. F. de Moura, A. V. Malyshev, M. L. Lyra, V. A. Malyshev, and F. Dominguez-Adame, “Localization properties of a one-dimensional tight-binding model with nonrandom long-range intersite interactions,” *Phys. Rev. B* **71**, 174203 (2005).
- [76] Janos Perczel and Mikhail D Lukin, “Theory of dipole radiation near a dirac photonic crystal,” (2018), [arXiv:1810.12815](https://arxiv.org/abs/1810.12815).
- [77] A. González-Tudela and J. I. Cirac, “Exotic quantum dynamics and purely long-range coherent interactions in dirac conelike baths,” *Phys. Rev. A* **97**, 043831 (2018).
- [78] Raj Pandya, Richard Chen, Qifei Gu, Jooyoung Sung, Christoph Schnedermann, Oluwafemi S Ojambati, Rohit Chikkaraddy, Jeffrey Gorman, Gianni Jacucci, Olimpia D Onelli, *et al.*, “Ultrafast long-range energy transport via light-matter coupling in organic semiconductor films,” (2019), [arXiv:1909.03220](https://arxiv.org/abs/1909.03220).

Appendix A: Finite-size analysis of the numerical data

In this Supplemental Note we provide additional data on finite-size scaling and extrapolation procedure for the numerical data.

1. Finite-size flow of the ratio r -statistics

First, we describe the procedure of the finite-size collapse of the ratio r -statistics. For each value of the bare hopping decay rate a the ratio r -statistics has been calculated for the range of anisotropy parameters β and system sizes L (see Fig. 3(a) in the main text for $a = 1$).

The first approximation of the transition $\beta = \beta_{AT}(a)$ is given by the crossing point of finite-size $r(\beta, N)$ curves, see Fig. 3(a). More accurate single-parameter collapse of all curves of the form

$$\langle r \rangle(\beta, L) = R(|\beta - \beta_{AT}|L^{1/\nu}) \quad (\text{A1})$$

provides best parameters β_{AT} and ν , see Fig. 3(b).

The black solid line in Fig. 1 in the main text shows the result for the critical value of β_{AT} which coincides with the analytical prediction, Eqs. (2-3), within the $\sim 10\%$ -errorbar.

2. Extrapolation of the multifractal spectrum $f(\alpha)$ and fractal dimensions D_q

In this subsection we provide the standard extrapolation procedure for the spectrum of fractal dimensions (see, e.g., [14, 15, 20, 35, 36]) and for the fractal dimensions D_q [23].

For the former we use the following expression for the multifractal spectrum $f(\alpha, N)$ at finite system size $N = L^d$, $d = 2$

$$f(\alpha, N) = f(\alpha) + \frac{c_\alpha}{\ln N}, \quad (\text{A2})$$

with a certain α -dependent constant c_α . This follows from the definition of the multifractal spectrum $f(\alpha)$ given by the scaling of the probability distribution $\mathcal{P}(\ln |\psi_n(i)|^2) \sim N^{f(\alpha)-1}$ of the logarithm of the wavefunction intensity $\alpha = -\ln |\psi_n(i)|^2 / \ln N$ [23] and extracted directly from the histogram over α [35–37].

The corresponding finite-size $f(\alpha, N)$ and extrapolated $f(\alpha)$ curves are given in Fig. 6 for a certain mid-spectrum energy $E = 5$ in the localized phase, $a = 1.5$, $\beta = -1$ and obey the normalization condition, $\max_\alpha f(\alpha) = f(\alpha_0) = 1$, of the probability distribution $\mathcal{P}(\alpha)$.

The position of the maximum α_0 of $f(\alpha)$ and its slope $k = 1/\alpha_0$ corresponds to the effective power-law spatial decay of the wavefunction with the distance $r = |i - i_0|$ from its maximum $i = i_0$. Indeed, with the distance the eigenstate decays as $N^{-\alpha} = |\psi_n(i)|^2 \sim r^{-\gamma(a)}$,

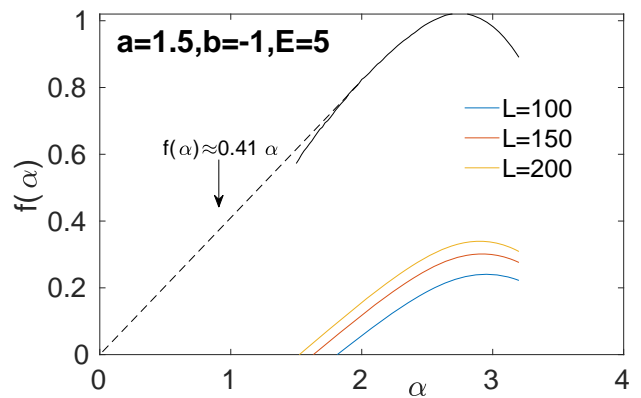


FIG. 6. **Finite-size extrapolation of the multifractal spectrum** $f(\alpha)$ for the energy $E = 5$, disorder strength $W = 10$, $a = 1.5$, and $\beta = -1$. $f(\alpha)$ is extrapolated from $L = 100, 150$, and 200 with the corresponding number of disorder realizations $1000, 500$, and 100 , respectively.

$\gamma(a) = 2 \max(a, 2d - a)$, while the number of states increases as the volume $N^{f(\alpha)} \sim r^d$. Thus, resolving these expressions with respect to r one obtains

$$f(\alpha) = \frac{\alpha}{\alpha_0}, \quad \alpha_0 = \frac{\gamma(a)}{d} = \max(a, 2d - a), \quad (\text{A3})$$

which is confirmed by the numerical simulations, Fig. 6.

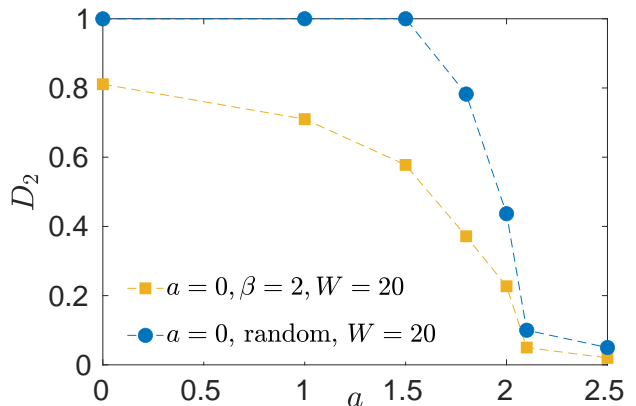


FIG. 7. **Comparison of extrapolated D_2 versus a** for the anisotropic model with fixed bare disorder $W = 10$ (yellow squares) and for the $2d$ power-law random banded model (blue circles). The anisotropy is taken to be $\beta = 2$. D_2 are extrapolated from $L = 100, 150, 200$, and 250 with the corresponding number of disorder realizations $1000, 500, 100$, and 50 , respectively.

The finite-size fractal dimension is defined by the formula $D_q(N) = \ln I_q / (1 - q) \ln N$, with the generalized inverse participation ratio (IPR), $I_q = \langle \sum_i |\psi_n(i)|^{2q} \rangle = c_q N^{(1-q)D_q}$. Main contributions to it are given by the scaling exponent D_q and the prefactor c_q of IPR simi-

larly to (A2)

$$D_q(N) = D_q + \frac{(1-q)^{-1} \ln c_q}{\ln N}. \quad (\text{A4})$$

The resulting extrapolated D_2 is shown in Fig. 7 versus a for $\beta = 2$. One can see there (yellow squares) the transition from localized phase $a > 2$ with $D_2 \rightarrow 0$ to the extended one, $D_2 > 0$, at $a < 2$. As a reference point we show the fractal dimension for the power-law random banded matrix (PLRBM) model [23] extrapolated using the simple linear formula (A4). The discrepancy between these models in the extended phase is due to severe finite-size effects in anisotropic model (we address this issue in the next Supplemental Note).

3. Inverse participation ratio and the fraction of ergodic states

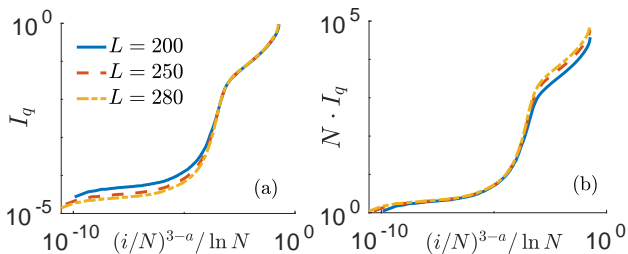


FIG. 8. Inverse participation ratio sorted in increasing order versus renormalized state index (a) IPR itself showing collapse at the localized states and (b) IPR renormalized to the system size N showing the collapse for ergodic states. The disorder strength for $a = 1$, $\beta = 0.3$ is $W = 20$. Finite size data is represented for $L = 200$ (solid blue), 250 (dashed red), and 280 (dash-dotted yellow) with the corresponding number of disorder realizations 100, 80, and 50, respectively.

Here we focus on the estimation of the fraction of ergodic high-energy states in the localized state at $0 < \beta < a < 2$. In order to check Eq. (8) of the main text we consider the plot of energy-dependent IPR values sorted in increasing order for different system sizes versus the renormalized fraction of the states $(n/L)^{3-a}/\ln L$, see Fig. 8. Panels (a) and (b) show the IPR itself I_q and its renormalization $N \cdot I_q$ in order to emphasize the scaling of the localized and ergodic states, respectively, given as an inset to Fig. 3(b) in the main text. The same analysis has been done for the ratio r -statistics versus energy (not shown) based on Fig. 2(b).

Appendix B: Numerical characterization of extended phase

In this Supplemental Note we characterize the extended phase of the considered anisotropic model using more quantities from the multifractal analysis.

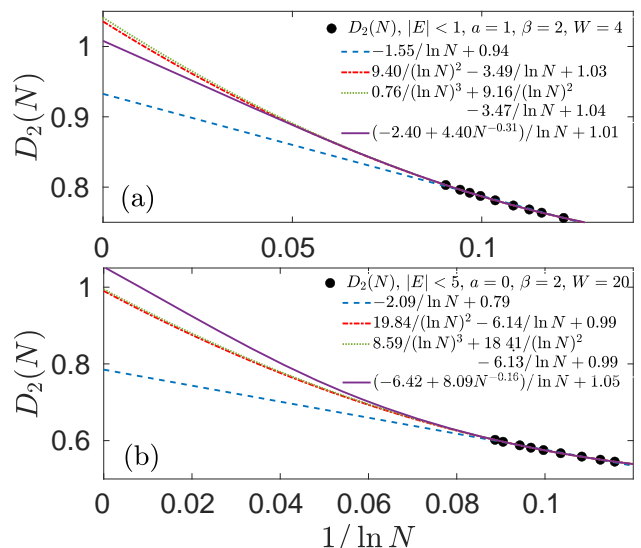


FIG. 9. Finite-size extrapolation of the fractal dimension D_2 (symbols) with linear (blue dashed), quadratic (red dash-dotted), cubic (green dotted) expressions in $x = 1/\ln N$ as well as the one with irrelevant exponent (violet solid) considered in [61]. We show two parameter sets (upper panel) $a = 1$, $\beta = 2$ is $W = 4$ and (lower panel) $a = 0$, $\beta = 2$ is $W = 20$ in order to emphasize that this issue present both at weak and strong disorder. D_2 is averaged over the energy interval $|E| < W/4$ and extrapolated from $L = 75, 85, 100, 125, 150, 175, 200,$ and 250 with the corresponding number of disorder realizations 2000, 2000, 2000, 2000, 1000, 600, 600, and 300, respectively.

First, we should mention that the extrapolation of D_2 in this case is more subtle. Due to limited system sizes in 2d the linear approximation (A4) provides unreasonable results and, thus, following recent literature we use quadratic in $1/\ln N$ extrapolation and compare it with further cubic one both for weak and strong disorder, see Fig. 9. In order to double check we also fit the data with the expression with irrelevant exponent suggested in [61]

$$D_q(N) = D_q + \frac{(1-q)^{-1} \ln c_q + \gamma_q N^{-y_{irr}}}{\ln N}. \quad (\text{B1})$$

All the results confirm the ergodic nature of the extended phase in the considered model which is spoiled by severe finite-size effects forcing one to go beyond linear extrapolation, Eq. (A4).

1. Finite-size behavior of the wave function decay

The wave function spatial decay at several system sizes shows that in the extended phase the power-law decay with dual decay rate $\gamma(a) = 2 \max(a, 2d - a)$ develops only at small distances $|i - i_0| \equiv r < r_0 \sim L^m$ which increases with the system size slower than the lengthscale, $m < 1$, Fig. 10 At larger distances the power-law tail

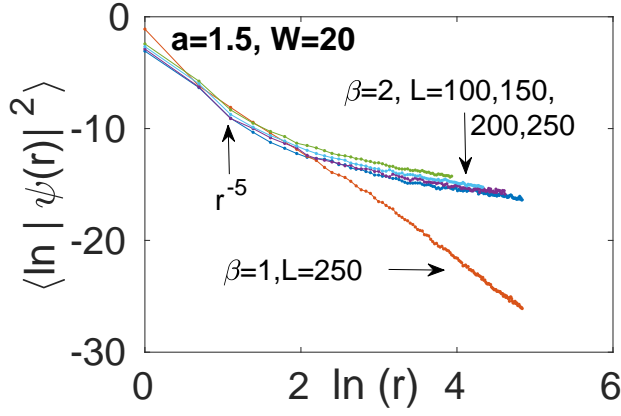


FIG. 10. **Spatial wave function decay in the extended phase**, $a = 1.5$, $\beta = 2$, for different system sizes. in comparison to the one in the localized phase (red line), $a = 1.5$, $\beta = 1$. The disorder strength is taken to be $W = 20$. System sizes are $L = 100, 150, 200$, and 250 with the corresponding number of disorder realizations 1000, 500, 100, and 50, respectively.

with smaller decay rate $c \leq d$ grows

$$|\psi_n(i)|^2 \sim \begin{cases} L^{-A} \left(\frac{r}{r_0}\right)^{-\gamma(a)}, & r < r_0 \\ L^{-A} \left(\frac{r}{r_0}\right)^{-c}, & r > r_0 \end{cases} \quad (\text{B2})$$

and eventually it leads to the decay of the wave function maximum $|\psi_n(i_0)|^2 \sim L^{\gamma m - A}$, which is consistent with the ergodic typical value $|\psi_n(L)|^2 \sim L^{-A - (1-m)c} \sim L^{-d}$, as $A = d - (1-m)c$, confirming, thus, Fig. 4(a) of the main text. In the Fig. 10 we have $c \simeq 1$, $A - \gamma m \simeq 0.54$, with $m \simeq 0.12$.

2. Higher-order level statistics

Another interesting measure is the higher order of the ratio r -statistics [62, 63] generalizing the standard one [28, 29]. Indeed, the probability distribution $P(s, n)$ of the level spacing $s_{k,n} = (E_{k+n} - E_k)/\delta$ of the n -consecutive energies separated by $n-1$ levels in between, renormalized by the mean level spacing $\delta = \langle E_{k+1} - E_k \rangle$, both in the Wigner-Dyson and Poisson limit gives the same mean value $s = n$ while its variance determines the level rigidity and scales as $\sim \ln n$ ($\sim n$) for Wigner-Dyson (Poisson) case.

The analysis of the above distribution $P(s, n)$ in the extended phases of PLRBM and considered anisotropic model shows the Wigner-Dyson behavior of the former level rigidity and the Poisson scaling of the variance for the anisotropic non-random hopping case, Fig. 11(a-b).

The corresponding r_n -statistics,

$$r_n = \left\langle \frac{\min(s_{k,n}, s_{k+1,n})}{\max(s_{k,n}, s_{k+1,n})} \right\rangle \quad (\text{B3})$$

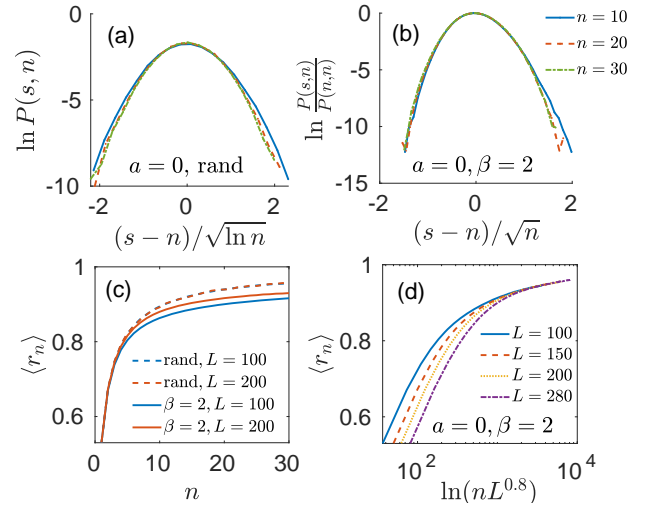


FIG. 11. **Higher-order level spacing distribution $P(s, n)$ and ratio level statistics r_n** . Upper row shows the collapse of $P(s, n)$ for different n (shown in legend) for (a) the $2d$ power-law random banded model showing Wigner-Dyson variance $\sim \ln n$, and (b) the anisotropic model showing Poisson level variance $\sim n$ at large $n \gtrsim 10$. Lower row shows the collapse of ratio r -statistics for different system sizes L (shown in the legend) (c) at small n (in the whole interval) for the anisotropic model [solid] (PLRBM [dashed]), and (d) at large $n \gtrsim 60$ for the anisotropic model by the rescaling of n to $nL^{0.8}$. In both models $a = 0$ and $W = 20$. In the anisotropic model $\beta = 2$. The number of disorder realizations is 1000, 500, 100, and 50 for $L = 100, 150, 200$, and 280, respectively.

of the considered anisotropic model shows Wigner-Dyson behavior at small $n \lesssim 5$ (cf. solid lines and the dashed one in Fig. 11(c)) and values consistent with Poisson at large $n \gtrsim 60$ after rescaling $nL^{0.8}$.

3. Overlap correlation function $K(\omega)$ and the correspondence to fractal dimensions

The overlap correlation function

$$K(\omega = E_n - E_{n'}) = N \sum_i \langle |\psi_n(i)|^2 |\psi_{n'}(i)|^2 \rangle \quad (\text{B4})$$

is an important measure of the wave function statistics [64, 65]. It is the Fourier-transform of the return probability [66–68] which is an important dynamical measure relevant also for many-body localization [69, 70].

The power-law decay rate $1 - D_s$ of $K(\omega)$ at small ω is usually related to the fractal dimension D_2 [71–73]

$$D_s = D_2, \quad (\text{B5})$$

however, in later works [36, 66, 74] this statement was generalized to the following: if the position of the crossover between two different power-law decays at small and large frequencies (associated with the mini-band size [36, 66]) does not scale with N , Eq. (B5) is valid [74].

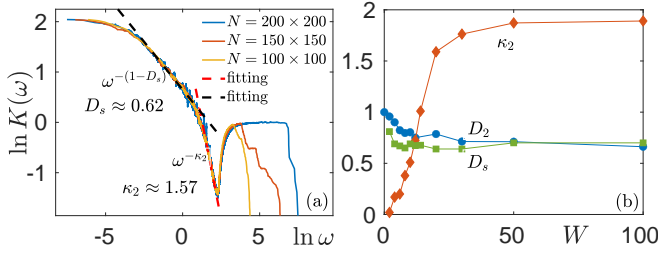


FIG. 12. **Overlap function $K(\omega)$ and the comparison of its decay rates to fractal dimensions D_2 .** (a) $K(\omega)$ for different system sizes L (shown in legend) in log-log scale. The power-law fitting gives $K(\omega) \sim \omega^{-\kappa}$, with $\kappa = 1 - D_s$ (κ_2) for small (large) ω . The parameters are $a = 0$, $\beta = 2$, and $W = 20$. (b) the comparison of the decay rates $1 - D_s$ and κ_2 of $K(\omega)$ with the fractal dimension D_2 versus the disorder strength W corresponds to the Chalker scaling $D_2 = D_s$. D_2 , D_s , and κ_2 are extrapolated from $L = 100, 150, 200$, and 250 with the corresponding number of disorder realizations 1000, 500, 100, and 50, respectively.

In Fig. 12 we show the typical plot of $K(\omega)$ in the extended phase of the considered model. Following the Chalker scaling, Eq. (B5), D_s is shown to be close to D_2 , while the decay rate κ_2 at larger ω approaches the dimensionality $\kappa_2 \rightarrow d = 2$ with increasing effective disorder according to [74].

Appendix C: Spectrum of hopping, Eq. (5)

The spectrum of the hopping term $V_{ij} = -\frac{1-\beta \cos^2 \phi_{ij}}{r_{ij}^a}$ from Eq. (1) is given by its Fourier transform due to translation-invariance of hopping

$$V_q = -\sum_{i,j} e^{iq_x(i_x-j_x)+iq_y(i_y-j_y)} \frac{1-\beta \cos^2 \phi_{ij}}{r_{ij}^a}. \quad (\text{C1})$$

For $a \neq d = 2$ the latter can be calculated in the continuous approximation as

$$V_q = -\int_0^\infty r dr \int_0^{2\pi} d\phi e^{iqr \cos(\phi-\phi_q)} \frac{1-\beta \cos^2 \phi}{r^a} = c_a q^{a-2} [\beta - a - (2-a)\beta \cos^2 \phi_q]. \quad (\text{C2})$$

Here $c_a = \pi 2^{1-a} \frac{\Gamma(-a/2)}{\Gamma(a/2)}$, $\Gamma(a)$ is a Gamma-function, and $q = \pi n/L$ is the quantized momentum, with integer $n \lesssim L/a_0$, a_0 is the inter-atomic distance which we choose to be unity $a_0 \equiv 1$ without loss of generality. The special case of $a = d = 2$ should be considered separately as the result depends explicitly on a_0

$$V_q = \pi \left[(2-\beta)(\gamma_E + \ln(qa_0/2)) - \frac{\beta}{2} \cos(2\phi_q) \right], \quad (\text{C3})$$

with the Euler - Mascheroni constant $\gamma_E \simeq 0.577216$.

The divergence of both Eqs. (C2) and (C3) at $q \rightarrow 0$ at $a \leq d$ signals on the presence of (the measure zero of) high-energy delocalized states [15, 21].

Appendix D: Main idea of the renormalization group analysis

In this Supplemental Note we follow [13, 21] and reproduce the idea of the renormalization group (RG) analysis for the 2d anisotropic system. Similarly to [13] let's take the disorder amplitude $W \gg 1$ to be large compared to the nearest-neighbor hopping $V_{i,i+1}$ and apply the RG procedure to study this problem. As a step of the RG we first cut off the tunneling at a certain scale R_0 and calculate the wavefunctions (R_0 modes) for this scale. Then new cutoff $R_1 \gg R_0$ is chosen and new modes (R_1 modes) are constructed as a superposition of R_0 modes. The localization length increases from $\ell_0 \lesssim R_0$ to $\ell_1 \lesssim R_1$ due to the presence of resonances. Due to the presence of large parameter $W \gg 1$ only pairs of resonances are taken into account (please see [21] for more details). The annihilation operators $\hat{\psi}_k^{(1)}$ of new R_1 modes can be written via the initial site annihilation operators \hat{c}_m as follows

$$\hat{\psi}_k^{(1)} = \sum_i \psi_k^{(1)}(i) \hat{c}_i. \quad (\text{D1})$$

Thus, the hopping term $V_{ij} = -\frac{1-\beta \cos^2 \phi_{ij}}{r_{ij}^a}$ rewritten in new operators takes the form

$$\sum_{i,j} V_{ij} \hat{c}_i^\dagger \hat{c}_j = \sum_{k,l} \hat{\psi}_k^{(1)\dagger} \hat{\psi}_l^{(1)} \sum_{i,j} \psi_k^{(1)}(i) \psi_l^{(1)*}(j) V_{ij}. \quad (\text{D2})$$

According to RG assumption the modes $\psi_k^{(1)}(m)$ are localized $r_{km} < \ell_1$ at the length $\ell_1 \lesssim R_1$, thus, one can neglect the difference between V_{ij} and V_{kl} ($|r_{ij} - r_{kl}| < r_{ik} + r_{jl} < 2\ell_1 \lesssim R_1$). As a result, Eq. (D2) reads as

$$\sum_{i,j} \frac{\hat{c}_i^\dagger \hat{c}_j}{r_{ij}^a} \simeq \sum_{k,l} \frac{t_0 l_k l_l^*}{r_{kl}^a} \hat{\psi}_k^{(1)\dagger} \hat{\psi}_l^{(1)}, \quad (\text{D3})$$

with the effective charge $l_k = \sum_i \psi_k^{(1)}(i)$.

In order to estimate the renormalized hopping term $l_k l_l^*/r_{kl}^a$ let's consider the mean squared value of l_k at a certain energy E as follows

$$\begin{aligned} \langle l^2 \rangle_E &= \frac{\langle \sum_k l_k^2 \delta(E - E_k) \rangle}{\rho(E)} = \\ &= \frac{\langle \sum_k \sum_{i,r_{ik} < R_1} \sum_{j,r_{jk} < R_1} \psi_k^{(1)}(i) \psi_k^{(1)*}(j) \delta(E - E_k) \rangle}{\rho(E)} \simeq \\ &= \frac{\sum_{r_{ij} < R_1} \langle \text{Im } G_{i-j} \rangle}{\rho(E)} \simeq \frac{\text{Im } \bar{G}_{q \simeq 1/R_1}(E)}{\rho(E)}, \quad (\text{D4}) \end{aligned}$$

Here the density of states (DOS) is given by

$$\rho(E) = \left\langle \sum_k \delta(E - E_k) \right\rangle = \frac{1}{N} \sum_q \text{Im } \bar{G}_q(E). \quad (\text{D5})$$

Taking into account that the imaginary part of the Green's function is given by a Lorentzian

$$\text{Im } \bar{G}_q(E) \simeq \frac{W}{(E - V_q)^2 + \pi W^2/12}, \quad (\text{D6})$$

in the coherent potential approximation, one can straightforwardly find that the DOS is q -independent and is determined solely by the disorder amplitude (like in [21])

$$\rho(E) \simeq \int \frac{d^d q}{(2\pi)^d} \frac{W}{(E - t_0 q^{a-d})^2 + W^2} \simeq \frac{1}{W}. \quad (\text{D7})$$

Here we consider for simplicity the box distribution of the disorder $-W/2 < \mu_i < W/2$ with the finite variance $\langle \mu_i^2 \rangle = W^2/12$ and use it in the determination of the self-energy of the Green's function.

As a result

$$\text{Im} \bar{G}_{q \sim 1/R_1}(E) \simeq \frac{W}{R_1^{2(d-a)}}, \quad (\text{D8})$$

and the effective hopping within the RG approximation scales as

$$V_R^{eff} = \min \left(\frac{t_0}{R^a}, \frac{W^2}{t_0 R^{2d-a}} \right). \quad (\text{D9})$$

giving localization with the characteristic change of the power law tail at $R \simeq W^{1/(d-a)} \gg 1$.

Eventually in the case $W \gg 1$ this estimate provides the localization of all eigenstates at $E \lesssim W \sim O(1)$ and the duality of the polynomial decay rate of the corresponding wave functions, $a_{eff} = \max(a, 2d-a)$ at $a < d$ and $a > d$. For more rigorous consideration of RG procedure, please see [13, 21].

Appendix E: Ioffe-Regel criterion

In this Supplemental Note we estimate the energy-dependent mean-free path for $a < d$ and apply the Ioffe-Regel criterion of localization in order to estimate the fraction of ergodic states in the localized phase of the considered anisotropic model.

The mean-free path at a certain energy E can be estimated as follows

$$\ell_{mfp}(E) \simeq v_{qE} \tau_{qE}, \quad (\text{E1})$$

where qE and v_q are determined from the following equations

$$V_{qE \lesssim 1} = E, \Rightarrow qE \sim \min \left[1, E^{-1/(d-a)} \right] \quad (\text{E2})$$

$$v_q = \frac{dV_q}{dq} \sim q^{a-d-1}, \quad (\text{E3})$$

while the level broadening can be estimated with Fermi Golden rule of the scattering of plane waves on the impurities $\mu_i \sim W$

$$\tau_{qE}^{-1} = \text{Im} G_{i-j=0}(E) \simeq \rho(E) \frac{W^2}{12}. \quad (\text{E4})$$

Small qE corresponds to large energies $E \gg W$, thus, the DOS at such energies is not anymore determined by (D7), but involves qE as follows

$$\rho(E \gg W) = \frac{d^d q_E}{dV_{qE}} \sim q_E^{2d-a}. \quad (\text{E5})$$

As a result using (D7) we obtain

$$\ell_{mfp}(E) \sim W^{-2} q_E^{2a-3d-1} \sim W^{-2} E^{(3d+1-2a)/(d-a)}. \quad (\text{E6})$$

According to the Ioffe-Regel criterion the states are delocalized

- in $d = 1$ as soon as $\ell_{mfp} > L$;
- in $d = 2$ as soon as $\ell_{loc} \sim e^{cqE \ell_{mfp}} > L$;
- in $d = 3$ as soon as $qE \ell_{mfp} > 1$.

leading to a certain upper cutoff $qE < q_*$. The fraction of such delocalized states is given by

$$f_{erg} = \int_0^{q_*} d^d q \sim q_*^d. \quad (\text{E7})$$

After straightforward algebra the mobility edge can be estimated as

- in $d = 1$

$$qE < q_* = (W^2 N)^{-\frac{1}{2(2-a)}} \Rightarrow f_{erg} \sim q_* \sim N^{-\frac{1}{2(2-a)}}; \quad (\text{E8})$$

- in $d = 2$

$$qE < q_* = (W^2 \ln N)^{-\frac{1}{2(3-a)}} \Rightarrow f_{erg} \sim q_*^2 \sim \ln N^{-\frac{1}{3-a}}; \quad (\text{E9})$$

- in $d = 3$

$$qE < q_* = W^{-\frac{2}{9-2a}} \Rightarrow f_{erg} \sim q_*^3 \sim O(1). \quad (\text{E10})$$

In the 2d case considered in the main text (see the inset to Fig. 3(b)) the fraction of ergodic states decays as the power of the logarithm of N .

Note that following [15, 75] one can find the fraction of modes which are localized in the momentum q -basis. This condition is related to the level spacing $|V_{qE} - V_{qE+\pi/L}|$ to be of the order of the corresponding hopping

$$|V_{qE} - V_{qE+\pi/L}| \sim \frac{v_{qE}}{N^{1/d}} > \frac{W}{N^{1/2}} \quad (\text{E11})$$

which leads to

- in $d = 1$

$$qE < q^{**} = \left(\frac{N^{1/2} W}{t_0} \right)^{-\frac{1}{(2-a)}} \simeq q^* \quad (\text{E12})$$

- in $d = 2$

$$q_E < q^{**} = \left(\frac{W}{t_0}\right)^{-\frac{1}{3-a}} \ll q^* \quad (\text{E13})$$

- in $d = 3$

$$q_E < q^{**} = \left(\frac{W}{N^{1/6}t_0}\right)^{-\frac{1}{4-a}} \ll q^* . \quad (\text{E14})$$

Note that the localization in the momentum q -basis is more restrictive for all $d > 1$ as it provides the fraction of plane wave modes, while most of delocalized modes in $d \geq 2$ are of diffusive nature.

Appendix F: Related models and feasible experimental setup

Some similar models based on Eq. (1) are also considered numerically: for instance, the hopping model $t_{ij} = \cos(kr_{ij})/r_{ij}^a$ and the hopping model $t_{ij} = (1 + \eta_{ij})/r_{ij}^a$ with uncorrelated random η_{ij} . Unlike the considered

model, Eq. (1), these two models show only ergodic delocalized states when $a < d = 2$. However, extended states for $\beta > a$ with Wigner-Dyson statistics are also observed in the power-law Euclidean random matrix models when $a < d = 2$ (The details of calculation will be shown in further publications). Such matrix ensemble is generated from the uniform-random-distributed quantum dipoles in a square lattice. As an experimentally feasible setup one can consider a set of ions trapped in individual microtraps, which allows for arbitrary geometries and easy control over the effective anharmonicity of the spatial ion motion near the microtrap minima. Spin-dependent optical dipole forces applied to such ionic crystal create long-range effective spin-spin interactions and allow the simulation of spin Hamiltonians that possess nontrivial phases and dynamics. By tailor the optical forces one can generate arbitrary interactions between spins. Our findings could be observed in the flip-flop spin-model, as well as in the phonon hopping model itself.

Another way to realize long-range anisotropic model would be to use the dipole radiation in a 2d photonic crystal near the Dirac cone (i.e., dipolar interaction mediated by the photonic Dirac cone between atoms), see Ref. [76] in which the authors obtain effective long-range interactions $1/r^{1/2}$, based on the results of Ref. [77]. The $1/r$ hopping $(\delta_{ab} - n_a n_b)/r$ can be as well relevant for 2d polaritons [78].